www.czasopisma.pan.pl PAN POLSKA AKADEMIA NAUK www.journals.pan.pl

Arch. Min. Sci. **67** (2022), 2, 239-258

Electronic version (in color) of this paper is available: http://mining.archives.pl

DOI: https://doi.org/10.24425/ams.2022.141456

WEI CHEN[1,2,3], HAI-LIANG XU[2,3*], BO WU[2,3*], FANG-QIONG YANG[2,3]

STUDY ON THE THREE-PHASE FLOW OF THE WATER TRANSFER EXPORT ELBOW OF NATURAL GAS HYDRATE

The Euler multiphase flow and population equilibrium model were used to simulate the three-phase flow field in the bubble expansion stage of the outlet curved pipe section. The influence of the ratio of the bending diameter and the volume fraction of the gas phase on the pressure loss is revealed, and the safety range of the optimum bending diameter ratio and the volume fraction of the outlet gas phase is determined. The results show that the three-phase flow in the tube is more uniformly distributed in the vertical stage, and when the pipe is curved, the liquid-phase close to the pipe wall gathers along the pipe flank to the outside of the pipe, the solid phase is transferred along the pipe flank to the inside of the pipe, and the gas phase shrinks along the pipe flank to the inner centre. The maximum speed of each phase of the three-phase flow in the elbow is at the wall of the tube from 45° to 60° inside the elbow, and the distribution law along the axial direction of the pipe is about the same as the distribution law of volume fraction. The pressure loss of the elbow decreases with the increase of the bend diameter ratio, when the bend diameter ratio increases to 6, the pressure loss of the pipe decreases sharply, and the pressure loss decreases slowly with the increase of the bend diameter ratio. When the gas phase volume score in the elbow reaches 70%, there will be an obvious wall separation phenomenon, to keep the system in a stable working state and prevent blowout, the gas phase volume score should be controlled within 60%.

Keywords: Deep-sea mining; Natural gas hydrates; Three-phase flow; Numerical simulation

[1] HUNAN UNIVERSITY OF HUMANITIES, DEPARTMENT OF ENERGY AND ELECTRICAL ENGINEERING, SCIENCE AND TECHNOLOGY, LOUDI, HUNAN 417000, CHINA
[2] CENTRAL SOUTH UNIVERSITY, SCHOOL OF MECHANICAL AND ELECTRICAL ENGINEERING, CHANGSHA, HUNAN 410083, CHINA
[3] STATE KEY LABORATORY OF HIGH PERFORMANCE COMPLEX MANUFACTURING, CHANGSHA, HUNAN 410083, CHINA

* Corresponding author: xhl3187@126.com

Natural gas hydrate, also known as combustible ice, is considered to be the most ideal alternative energy source for the 21st century [1]. Currently, the most promising method for commercial exploitation of submarine gas hydrates is the cutter suction mining methods [2,3]. The cutter suction mining method is a kind of solid-state mining method, which is aimed at a digenetic hydrate deposit with a bare sea surface or a shallow cover layer. The schematic diagram of the mining system is shown in Fig. 1. The specific working process of the mining system is as follows [4].

Submarine mining vehicles rely on the front cutter head to break up the hydrate deposits and pipette them into the auxiliary pump. Under the action of the auxiliary pump, the granular hydrate is sent to the hose drawn by the buoyancy ball, and then the particles enter the main slurry pump. The high-power main slurry pump draws hydrates into vertical pipes of several kilometres. When it is lifted through the pipeline, the tube flow pressure is lowered and the temperature is raised. After reaching the critical surface, the hydrate begins to decompose part of the methane to make the fluid into a solid-liquid-gas three-phase flow. After flowing through the bend at the exit, it flows into the surface hydrate separator.

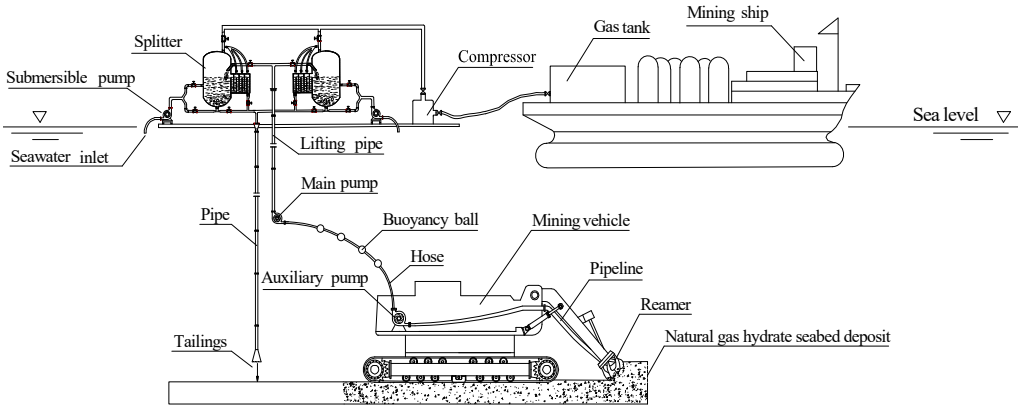

Fig. 1. Schematic diagram of submarine gas hydrate cutter suction mining system

The decomposition of hydrates makes solid-liquid two-phase flow transportation into solid-liquid-gas three-phase flow transportation, which is very likely to cause a blowout accident. Safe mining and pipeline transportation are important issues in gas hydrate mining. The study of gas hydrate decomposition sites and three-phase flow in hydraulic lifting pipelines is critical for safe mining [5,6].

In the study of the three-phase flow of natural gas hydrate pipeline, Wei et al. [7] used the method of hypothesis correction after indirect calculation and studied the problem of matching the structural parameters of the hot pipeline transportation in weather. Given the solid-state fluidisation mining scheme, Southwest Petroleum University Jiang et al. [8] and Zhou et al. [9] studied the gas hydrate sending gas to the ring air pipeline, modelled the process of bringing natural gas hydrate back to the sea through the ring air pipe after breaking, and obtained the multiphase flow characteristics of the ring air pipeline.

Afzali et al. [10], with the three-phase flow pipeline of oil and gas, studied different flow patterns corresponding to different pressure loss calculation methods. Li and Ma. [11] studied

the pressure loss of the three-phase flow segment of the pipeline. Li et al. [12], respectively, using the Euler model and CFD-PBM ("Computational Fluid Dynamics" Abbreviated as "CFD", "Population Balance Model" Abbreviated as "PBM") model for large gas phase volume fractions, hydraulically vertical pipe solid liquid gas three-phase flow simulation calculation.

The research on the flow state of elbow fluid is predominantly concentrated in the study of single-phase flow and two-phase flow. Zhan et al. [13] studied the distribution of velocity and pressure field in the elbow and carried out theoretical analysis and numerical simulation of the secondary flow (Dean vortex) of layer and turbulence. Su et al. [14] studied the wall separation phenomenon and its adverse effects of single-phase flow in the elbow flow field.

Natural gas hydrate is different from the traditional seafloor ore, it is formed under high pressure and low-temperature conditions, the pressure reduction and temperature increase will affect its balance so that it decomposes the natural gas. The decomposition of hydrates makes the two-phase flow transport of solid-liquid into solid-liquid gas three-phase transport, which can easily cause blowout accidents. Safe mining and transportation are important subjects in natural gas hydrate mining. Therefore, the research on the three-phase flow of natural gas hydrate pipelines is of great significance to safe exploitation [15].

1. Numerical simulation

1.1. Geometric models and meshing

The exit elbow is designed to be 90°, to make the curve ratio have sufficient value range and the three-phase flow before entering the bend ingesting segment to fully develop, the vertical segment axis and the exit plane distance is set to 5 m. The vertical segment axis and the inlet plane distance is set to 10 m. The centre of the bottom end of the curved pipe is the coordinate system origin. The vertical segment axis is in the direction of the Y-axis, and the horizontal segment axis is parallel to the X-axis.

The bend structure is simple, and a circular section O-type division is used along with a boundary layer that is encrypted by the Exponential rule, at which time the convergence speed and precision can meet the numerical calculation requirements. Fig. 2 shows the exit elbow model and the cross-section mesh division model.

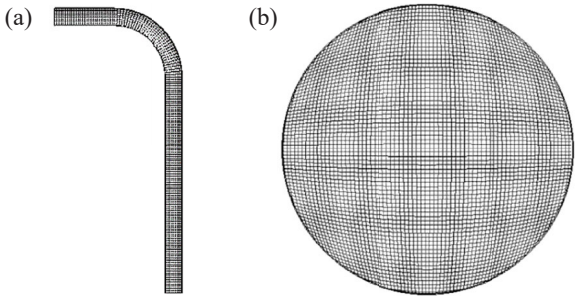

Fig. 2. Elbow model and cross-sectional enlarged view; (a) Elbow model, (b) cross-sectional enlarged view

1.2. Basic assumptions

According to the actual working conditions of the deep-sea mining system operation, combined with the principle of hydraulic transmission, the limitations of numerical calculation and the feasibility of regular analysis, the following assumptions are made:

(1) The solid phase and the liquid phase are continuous incompressible fluids. The gas phase obeys the R-K equation of state.
(2) The main phase is seawater, the secondary phase is hydrate deposit particles, and the third phase is methane. Both the solid phase particles and the gas phase bubbles are spherical.

1.3. Numerical simulation models and Governing equation

Due to the low pressure at the outlet elbow, the bubble volume fraction is large, the bubbles are concentrated and broken very violently to make the simulation more accurate, and the Euler Multiphase Flow and Population Balance Model (PBM) are selected. The CFD-PBM model is used to deal with bubble populations in three-phase flow, and in the solid-liquid gas system, the flow is in different flow patterns, depending on the apparent gas velocity and the apparent liquid velocity [16].

The bubble distribution, volume fraction and rising speed are all related to the bubble size, and the flow pattern is also closely related to the bubble size and distribution. Quantitative description of bubble size distribution is precisely the advantage of the PBM model. According to the bubble size distribution, the interaction between phases can be calculated, and the fluid flow state within different flow types can be more accurately simulated [17]. For the bubble expansion segment, the analysis of the bubbles selects the PBM model, which is mainly affected by the traction force, the additional mass force caused by the accelerated motion, the radial-lift force, the turbulent diffusion force and the wall lubrication force. The control equation is as follows.

The continuity equation for each phase is:

$$\frac{\partial\left(\rho_q\right)}{\partial t}+\frac{\partial\left(\rho_q \mathbf{u}_{q,i}\right)}{\partial x_i}=0 \tag{1}$$

where ρ is the density (kg/m^3); q is the phase code (g is the gas phase, l is the liquid phase, and s is the solid phase); t is the time (s); $\mathbf{u}$ is the velocity (m/s); and i is the coordinate direction.

Momentum equations for each phase is:

$$\frac{\partial\left(\rho_q \mathbf{u}_{q,j}\right)}{\partial t}+\frac{\partial\left(\rho_q \mathbf{u}_{q,i}\mathbf{u}_{q,j}\right)}{\partial x_i}=-\frac{\partial p}{\partial x_j}+\frac{\partial}{\partial x_i}\times\left(\sum_{q=1}^{n}\mu_q\right)\left(\frac{\partial \mathbf{u}_{q,i}}{\partial x_j}+\frac{\partial \mathbf{u}_{q,j}}{\partial x_i}\right)+$$
$$+\rho_q \mathbf{g}+\mathbf{F}_q+\frac{\partial}{\partial x_i}\sum_{k=1}^{n}\left(C_{vq}\rho_q \mathbf{u}_{D,q,i}\mathbf{u}_{D,q,j}\right) \tag{2}$$

where j is the phase component (kg/m^3); p is the pressure (Pa); μ is the viscosity (Pa·s); $\mathbf{g}$ is the Gravity acceleration (9.81 m/s^2); $\mathbf{F}_q$ is the unit mass force of fluid micelles (N/m^3); C_v is the volume fraction; and $\mathbf{u}_D$ is the slip speed (m/s).

Group balance equation [18]:

$$\frac{\partial n(v,t)}{\partial t}+\nabla\cdot[\mathbf{v}n(v,t)]=\frac{1}{2}\int_0^v a(v-v',v')n(v-v',t)n(v',t)dv'+$$
$$-\int_0^\infty a(v,v')n(v,t)n(v',t)dv'+\int_\Omega vb(v')\beta(v\mid v')n(v',t)dv'+$$
$$-b(v)n(v,t) \tag{3}$$

where $n(v,t)$ is bubble distribution function; $a(v,v')$ is bubble convergence and rate function; $b(v,v')$ is bubble Break Rate Function; $\beta(v,v')$ is a probability density function.

In the formula (3), the first item on the right represents "bubbles gather and generate", the second item on the right represents "bubbles gather and die", the third item on the right represents "bubble break generation", and the fourth item on the right represents "bubble breaks and dies".

Multiphase flow elbow transport is a swirl, and the RNG κ-ε model takes into account the rotation flow in the flow by correcting the turbulence viscosity [19], and the transport equation is:

$$\frac{\partial(\rho k)}{\partial t}+\frac{\partial(\rho k u_i)}{\partial x_i}=\frac{\partial}{\partial x_j}\left[(\alpha_k\mu_{eff})\frac{\partial k}{\partial x_j}\right]+G_k-\rho\varepsilon \tag{4}$$

$$\frac{\partial(\rho\varepsilon)}{\partial t}+\frac{\partial(\rho\varepsilon u_i)}{\partial x_i}=\frac{\partial}{\partial x_j}\left(\alpha_\varepsilon\mu_{eff}\frac{\partial\varepsilon}{\partial x_j}\right)+C_{1\varepsilon}^*\frac{\varepsilon}{k}G_k-1.92\rho\frac{\varepsilon^2}{k} \tag{5}$$

In the above formula:

$$\begin{cases} G_k=\mu_i\left(\dfrac{\partial u_i}{\partial x_j}+\dfrac{\partial u_j}{\partial x_i}\right)\dfrac{\partial u_i}{\partial x_j} \\ \mu_{eff}=\mu+\mu_t \\ C_{1\varepsilon}^*=1.42-\dfrac{\eta(1-\eta/4.377)}{1+0.012\eta^3} \\ \eta=\dfrac{k}{\varepsilon}\left(2E_{ij}\cdot E_{ij}\right)^{1/2} \\ E_{ij}=\dfrac{1}{2}\left(\dfrac{\partial u_i}{\partial x_j}+\dfrac{\partial u_j}{\partial x_i}\right) \end{cases}$$

In the above formula, k is turbulent energy, m^2/s^2; ε is turbulence dissipation rate; u is the average speed of time, m/s; G_k is effect of compressible turbulence pulsating expansion on total dissipation; α_k and α_ε are the inverses of the effective Prandtl number of turbulent energy k and turbulent dissipation ε, respectively.

Hydrates are decomposed and reach the sea soon after, and the reduction of large-grain hydrates in the pipeline is very small and negligible. Pipe pressure is reduced near the outlet, hydrate

decomposition accelerates, gas phase volume fraction increases bubbles (called bubble expansion segments), and the PBM model simulates the fragmentation and convergence of bubbles.

Setting model boundary conditions, the import boundary is the speed entry. The exit boundary is the pressure outlet. The wall boundary is a solid, non-slip wall surface. The PBM model divides bubbles into 5 groups, and the specific parameter settings are shown in Table 1.

TABLE 1

Elbow flow analysis parameters

Parameters	Unit	Numerical	Parameters	Unit	Numerical
Vertical tube length	mm	8000	Solid phase volume fraction	/	25%
Horizontal tube length	mm	3000	Gas phase volume fraction	/	10%
Pipe diameter	mm	500	Maximum diameter of bubbles	mm	16
Velocity	m/s	4	Bubble minimum diameter	mm	1
Bend ratio	/	4	Ratio Exponent	/	3
Solid phase diameter	mm	15	*Kv*	/	0.5236

1.4. Grid independence verification

To verify the influence of mesh size on the calculation results, four kinds of sizes were used to divide the pipeline model, and the corresponding mesh numbers were 0.36 million, 0.85 million, 1.12 million and 1.84 million. Selecting three points from the pipeline inlet 1 m, 2 m and 5 m in the model, and the specific coordinates of three points are M1 (0, 50, –1000), M2 (0, –50, –2000), M3 (0, 0, –50000). At the same working condition, using four kinds of meshes to simulate and analys e the solid phase concentration at three points.

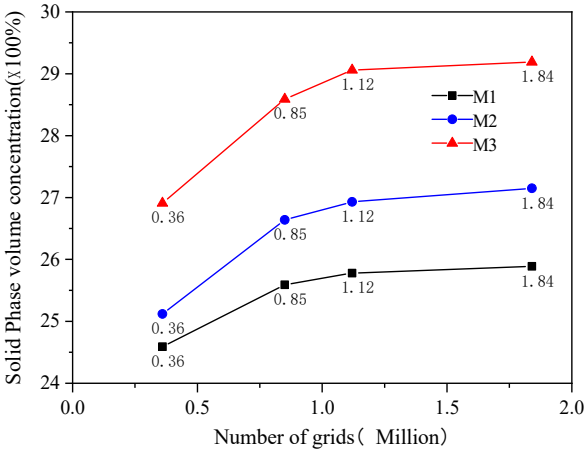

Fig. 3. Grid size-independent validation results

Hydrates are decomposed and reach the sea soon after, and the reduction of large-grain hydrates in the pipeline is small enough to be negligible. Pipe pressure reduces near the outlet,

hydrate decomposition accelerates, gas-phase volume fraction increases bubbles (called bubble expansion segments), and the PBM model simulates the fragmentation and convergence of bubbles.

Setting model boundary conditions, the import boundary is the speed entry. The exit boundary is the pressure outlet. The wall boundary is a solid, non-slip wall surface. The PBM model divides bubbles into 5 groups, and the specific parameter settings are shown in Table 1.

2. Analysis of numerical simulation results

2.1. Analysis of flow field in the exit elbow

Fig. 4 shows a cloud map of the volume fraction distribution of each phase on the pipeline XOY section. As can be seen from this graph, the phases are relatively evenly distributed in the vertical rise stage. When passing through the elbow, the state of motion is also different due to the different density and kinetic energy of each phase. In general, after the uniform fluid passes through the elbow into the horizontal segment, the solid liquid gas three phases are gradually layered according to the density size, the solid-phase is deposited downward, the liquid phase is concentrated in the middle of the pipeline, and the gas phase floats in the upper most layer.

Fig. 5 shows the volume fraction distribution cloud map at the point of the rising segment Y = 2 m, 4 m, 6 m, 8 m section of each phase. As can be seen from the figure, the particles and gases are attached to the pipe wall, and the liquid phase forms a clear water ring inside the gas-solid dense ring. When the particle phase speed and volume fraction are relatively low, the solid phase is easy to close to the pipe wall.

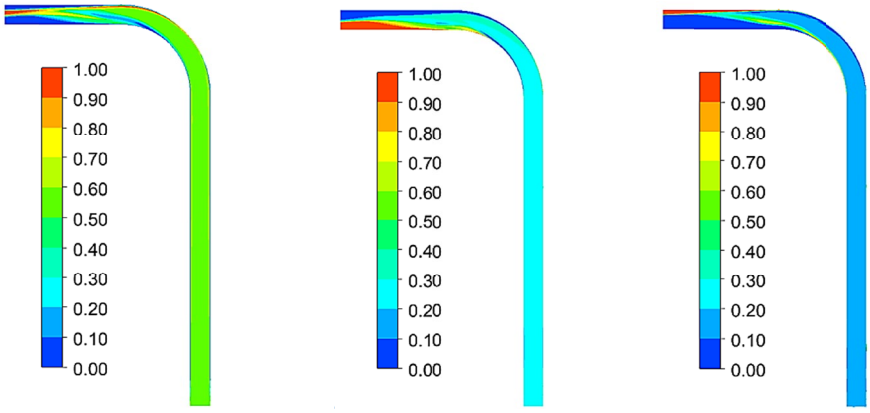

Fig. 4. Volume fraction on pipe XOY cross-section

Further analysis reveals that at Y = 8 m the clear water ring has shifted to the outside of the curved pipe (the outside of the circle in the figure is the outside of the pipe and the left side is the inside of the pipe), which indicates the beginning of the change in the distribution of each

phase. The outward offset of the clear water ring is also the thinning of the water ring on the outside of the elbow, and the water ring on the inside of the elbow becomes thicker, which is caused by the pipe bending to the inside and the external fluid being shifted to the inside, caused by the accumulation of the inner fluid.

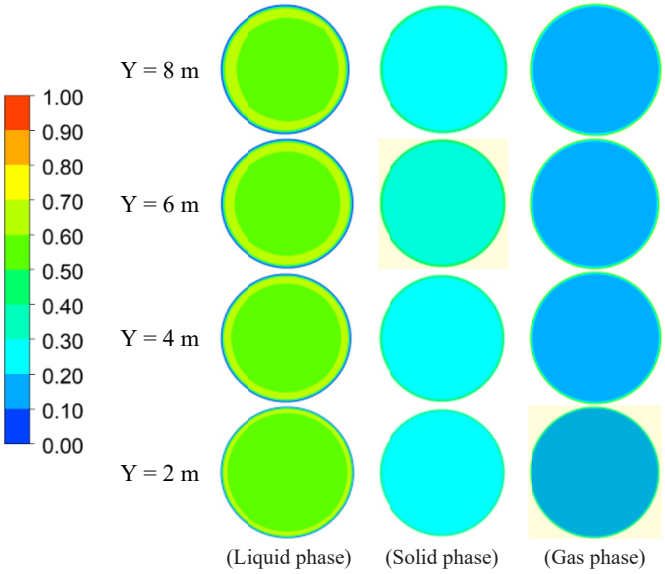

Fig. 5. From bottom to up Y-2,4,6,8 phase volume fraction distribution cloud

Fig. 6 shows the bending segments are 0°, 15°, 30°, 45°, 60°, 75°, 90°, of the cross-section at the volume fraction distribution cloud map. As can be seen from this figure: with the increase of angle, the liquid phase along the pipe flank gradually gathered to the outside of the pipe, forming a crescent. It is due to the mainstream direction of the fluid to the inner offset squeeze of the inner liquid of the pipe, the original direction of the inner liquid of the pipe is vertically upwards,

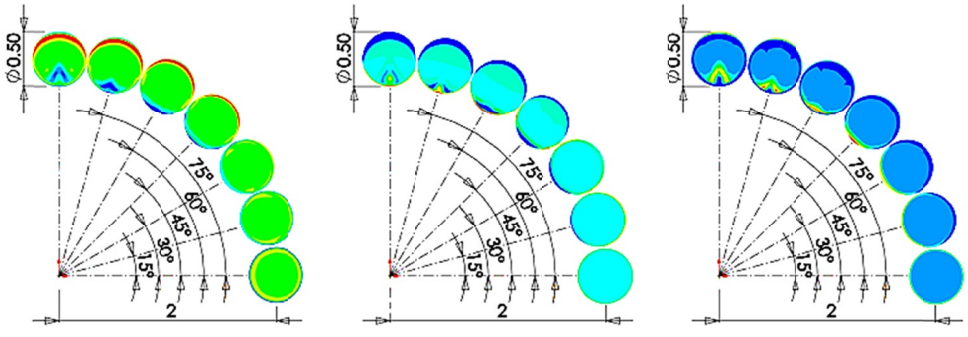

Fig. 6. Volume fractions of phases at each angle cross-section of the bending segment

due to the inertia, the direction of the liquid is still in upwards orientation, and the inner liquid to the flank of the shift resistance is small, so the liquid phases along with the pipe flank shift.

Before 45°, the liquid phase is gathered and close to the wall of the tube. After 45°, the liquid phase begins to detach from the pipe wall, but it is still crescent-like. There are two main reasons for the above phenomenon. The first reason is that at the 45° position, the outer pipe wall of the pipe collides with the liquid that shifts from the flank, causing the liquid to change direction. The second reason is that at a position above 45°, the adhesion of the outer pipe wall of the pipe to the liquid is not sufficient to cancel out the gravity of the liquid. So the liquid phase falls down.

The solid phase is gradually transferred along the pipe flank to the inside of the pipe, and when transferred to the inner centre, it begins to accumulate, showing an upright hill shape. This is because the solid phase is dense and gravity-heavy, tending to shift down to the lower side of the tilting pipe.

The gas phase is divided into two parts under the squeeze of the solid-liquid phase. Part of the part shrinks along the pipe flank toward the inner centre, squeezes it, slowly gathers toward the top of the solid phase. The other part is evenly distributed along the outside of the pipe and gradually gathers toward the pipe wall, presenting a small crescent-shaped gas-phase area at 90°.

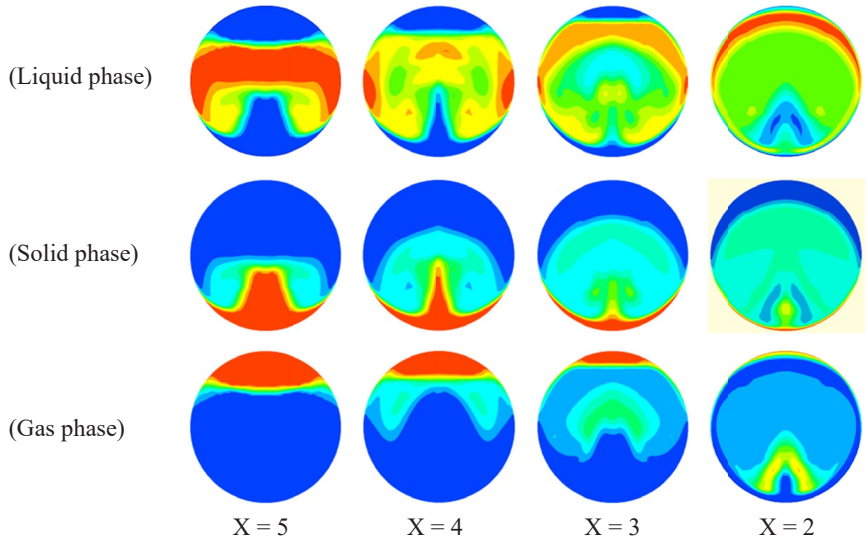

Fig. 7. Horizontal segments of each phase volume fraction cloud map

Fig. 7 is the map of the volume fraction distribution of each phase at the horizontal segment X-2, X-3, X-4, X-5 (exit). In the above paragraph, you can see the process of changing the redistribution of the phases in the pipeline. The solid phase is concentrated and deposited at the bottom of the pipe, the high concentration area grows to a certain height and gradually widens, and the upper contour of the sub-high concentration area is gradually flattened by the circle. The concentration of the left and right flank wall is lower than that of the middle region, which is caused by secondary flow.

A gas phase at the bottom of the pipe (inside the elbow) floats through the upper part of the pipe through the liquid phase above the solid phase and gradually converges on the top of the pipe (outside the elbow). The liquid phase is squeezed by the gas phase, which gathers from the top and bottom of the pipe to the middle, where the top is only squeezed by the gas phase, and the force is more uniform, so the level of the top of the liquid phase is slowly reduced. The bottom of the liquid phase is not only subject to the crowding of the solid phase, but also by the buoyancy of the gas phase, and the concentration distribution is affected by the gas phase through the liquid phase, more complex, in general, it will eventually reach the solid phase in the lower gas phase of the distribution. The inter-phase interface is affected by the secondary flow.

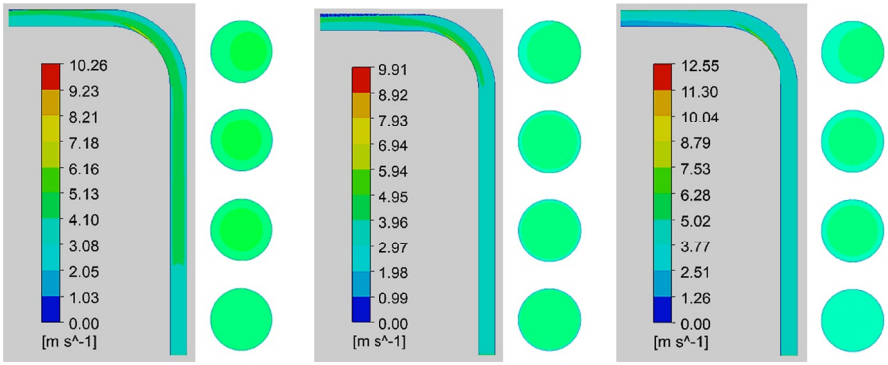

(Liquid phase) (Solid phase) (Gas phase)

Fig. 8. Pipe XOY cross-section and vertical section Y-2,4,6,8 phase speed

Fig. 8 is the phase velocity distribution map of the pipe XOY section and vertical segment (from bottom to top Y-2, Y-4, Y-6, Y-8) section. Fig. 9 is a phase velocity distribution map on the angle D section of the curved sections of the pipe. Fig. 10 is the phase velocity distribution chart on the cross- section of the pipe horizontal segment (X-2, X-3, X-4, and X-5).

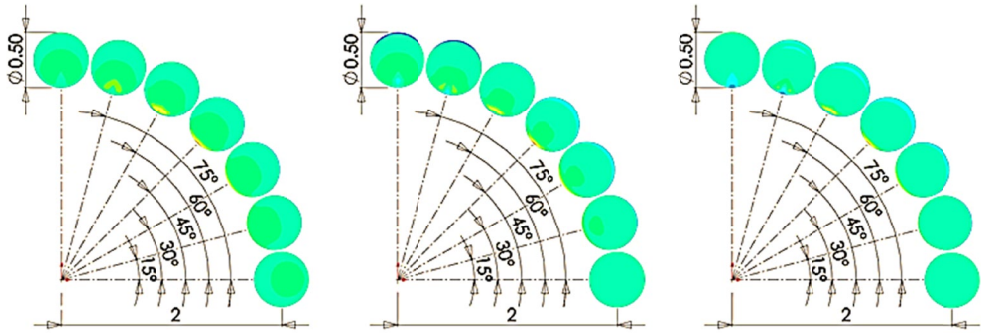

(Liquid phase) (Solid phase) (Gas phase)

Fig. 9. Phase speed at each angle section of the bending segment

As can be seen from Figs 8-10, the maximum speed of each phase is at the inside of the elbow at the wall of the pipe, 45° to 60°, and the speed in the middle of the pipe in the vertical rise stage is low. The high-speed zone of each phase of the bending stage moves from the outside to the inside and then offsets to the centre of the pipe. The two-phase velocity of the horizontal stage solid-fluid is concentrated in the middle, and the velocity distribution is about the same as the volume fraction distribution. The gas-phase velocity distribution is similar to that of solid-liquid but more uniform, with a speed difference of only 2.51 m/s.

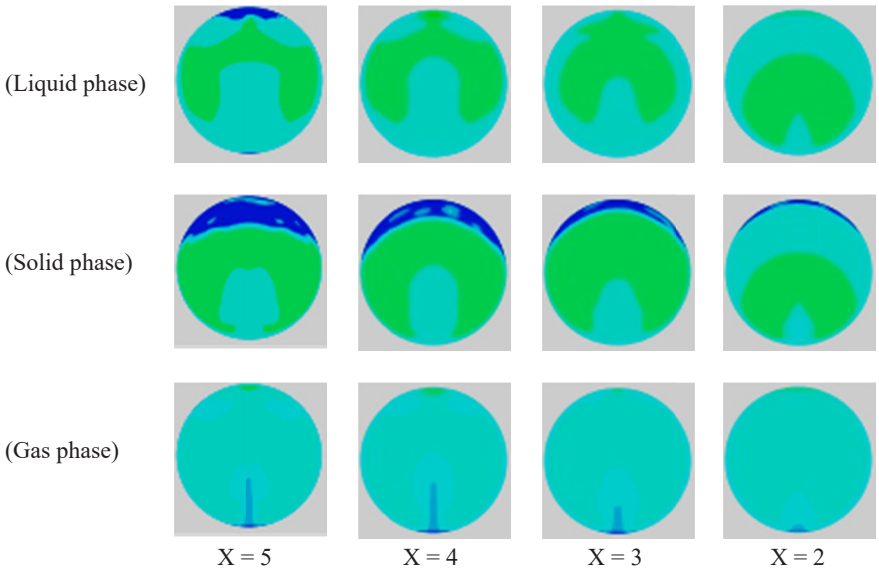

Fig. 10. Phase speed at each cross-section of the horizontal segment

2.2. Exit elbow secondary flow

Yin research shows that when the elbow transports a single-phase flow, at the entrance of the bending section, the mainstream speed near the inner wall of the pipe increases faster, so the secondary flow moves from the outer wall to the inner wall [20]. Due to the existence of secondary flow, the curved segment presents the phenomenon that the outer wall pressure is small and the inner wall is opposite. The secondary flow of the three-phase flow and the secondary flow of the single-phase flow have both similarities and differences. The formation, position and range of the vortex core are related to the radial velocity of each phase, also affecting the radial distribution of each phase.

Fig. 11 shows a flow of velocity flow between the curved segment and the three-phase flow in the horizontal segment pipe. The direction of the screenshot is reverse flow along the horizontal section of the pipe, the lower side connects the inner curvature of the curved segment, and the upper side connects the curved section curvature outside. As can be seen from the figure, at a position of 30°, the liquid phase on the left side of the pipe forms a vortex of a counterclockwise rotation and the vortex core that rotates clockwise on the right. As the elbow segment increases

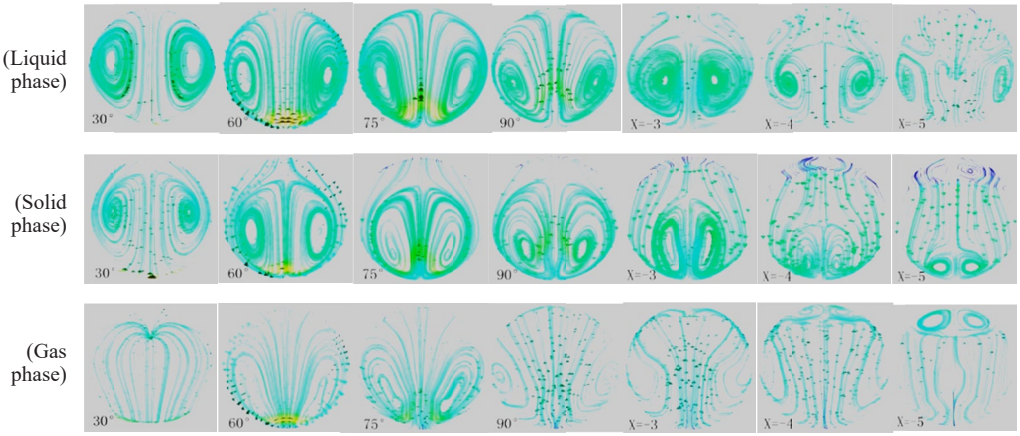

Fig. 11. Curved segments of each phase velocity flow chart

with the angle, the vortex core moves to the inside of the pipe, and the high-speed zone gradually gathers in the inner.

When the horizontal segment vortex core first gathers to the centre, the intensity increases, and then the offset strength to both sides weakens the position of the vortex core, and its influence area gradually decreases, the range gradually reduces. In this process, the upper part of the left and right vortex core begins to be connected, the middle uniform ascent becomes wider and begins to form a new vortex nucleus.

The solid phase is the same as the liquid phase, at a position of 30°, the left side of the pipe forms a vortex of counterclockwise rotation, and the right side forms a vortex core that rotates clockwise. In the elbow section, the solid-phase vortex core strength is slightly weaker, and the influence area is slightly smaller. When the bending angle is not large, the position of the solid phase and the liquid-phase vortex core is approximately the same, but after 60°, the position of the solid-phase vortex core is lower than that of the liquid-phase vortex core, which is related to the large concentration of solid phase and the greater impact of gravity. To the horizontal segment, the solid phase vortex core moves down to the lower part of the pipeline, and the scope of the impact area is reduced.

The gas-phase vortex nucleus is formed late, and only after 30° gradually forms a vortex of counterclockwise rotation on the left side of the pipe and a vortex core that rotates clockwise on the right. In the elbow section, the gas-phase vortex core is first elongated from a more rounded shape to the lower, and after 75°, the long striped vortex core begins to move to the left and right sides and gradually returns to the circle. After the horizontal segment, the left and right vortex cores gradually disappear, while a new vortex core appears at the top of the pipe, counterclockwise on the left and clockwise on the right.

2.3. Analysis of the effect of bend ratio to the flow field

The relative position of the elbow entrance and exit is unchanged, and the ratio of bend radius to the pipe diameter has a great effect on the three-phase flow.

Fig. 13 shows the volume fraction distribution of each phase at the exit section when r/d is 2, 4, 6, and 8 at a speed of 3 m/s. Compared with Fig. 12, it can be seen from the graph that the speed decreases and the solid phase deposition accelerates. This is because of the free settling speed of a

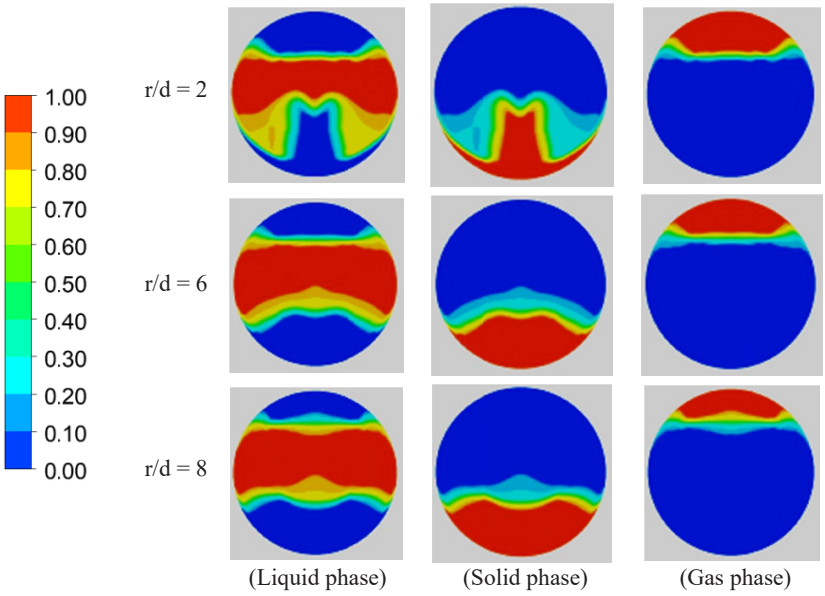

Fig. 12. At different bending diameter ratios, the volume fraction of each phase at the outlet (the speed is 4 m/s)

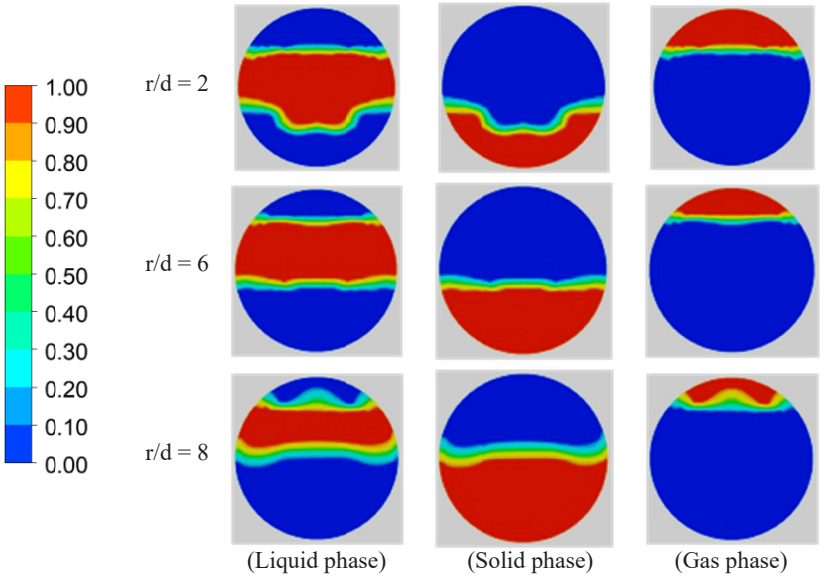

Fig. 13. The speeds is 3 m/s, the volume fractions of each phase at different bend sand s ratios

certain situation, where the transmission speed is small relative to the amount of settlement. The curve ratio is 2, the lower part of the liquid phase at the exit is raised, that is, the upper depression of the solid phase, because the original vortex at the outlet of the pipe is moving towards the pipe wall and gradually disappearing, the new vortex core appears in the middle and grows.

Fig. 14 is a line chart of the ratio of bend diameter to pipe pressure loss at speeds of 3 m/s, 4 m/s, and 5 m/s. From the figure, the pressure loss is relatively flat with the increase of the pipe bend ratio before the bend ratio is 5. When the curve ratio is between 5 and 6, the pressure loss decreases rapidly, and the pressure loss decreases slowly after 6, so the curve path ratio is reasonable compared to selecting 6.

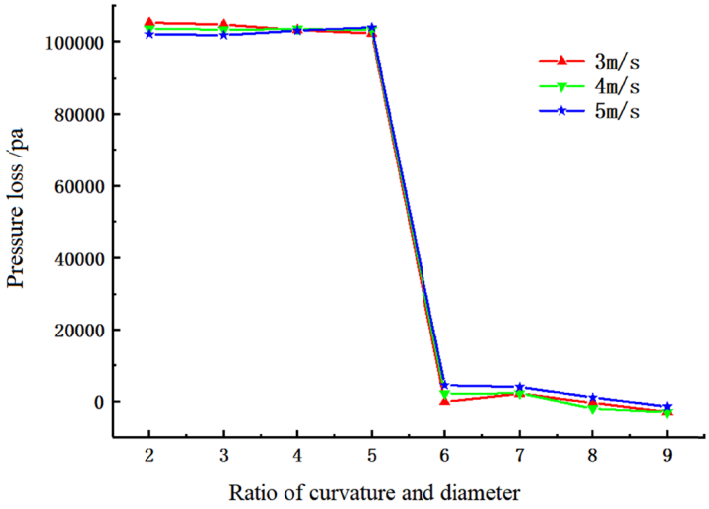

Fig. 14. Line chart of the relationship between pipe bend ratio and pressure loss

As can also be seen from Fig. 14, the pressure loss of the pipeline is not very different under different speed conditions. This is because the given entry has the same phase velocity, which can only be analysed if the decomposition critical surface is controlled at a higher position and the solid phase decomposition is small. In fact, when the solid phase decomposition occurs earlier, the decomposition is large, the distribution and speed of the phases before entering the elbow have been quite different. However, the gas phase speed is greater than the liquid phase speed, and the liquid phase velocity is greater than the solid phase speed. The specific situation is affected by the flow type transformation, export pressure, three-phase flow transmission distance and other factors and therefore relying on segment analysis is not good.

2.4. Analysis of the effect of gas phase volume fraction on flow field

Fig. 15 is a cloud map of the volume fractions of each phase at the piping XOY and outlet sections under the condition of the different gas phase volume fractions (50%, 60%, 70%). Through the XOY cross-section, it can be seen that, when the volume fraction is less than 60%, with the increase of gas-phase volume score, the solid phase particles gather more on the inside of the

bending segment, and the effect softens between them more violently. The separation degree of the two parts is more obvious in the liquid phase near the outer pipe wall and the liquid phase in the middle of the bending section of the pipe.

When the gas phase volume fraction continued to increase, the gas-solid two-phase in the rising segment near the inside of the pipe began to appear as an obvious wall separation phenomenon. This is because the increase in gas phase buoyancy becomes larger, the velocity of each phase increases, the turbulence energy increases, and the turbulence energy entering the rising section before the elbow is affected by it, reaching the critical value, so that the boundary layer is separated. At this point, the solid phase aggregation on the inside of the curved segment is gradually moving down. The appearance of the wall separation phenomenon will cause the sharp vibration of the pipe, and corrosion damage at the wall separation, should be avoided, thus it is best to control the export volume fraction within 60%.

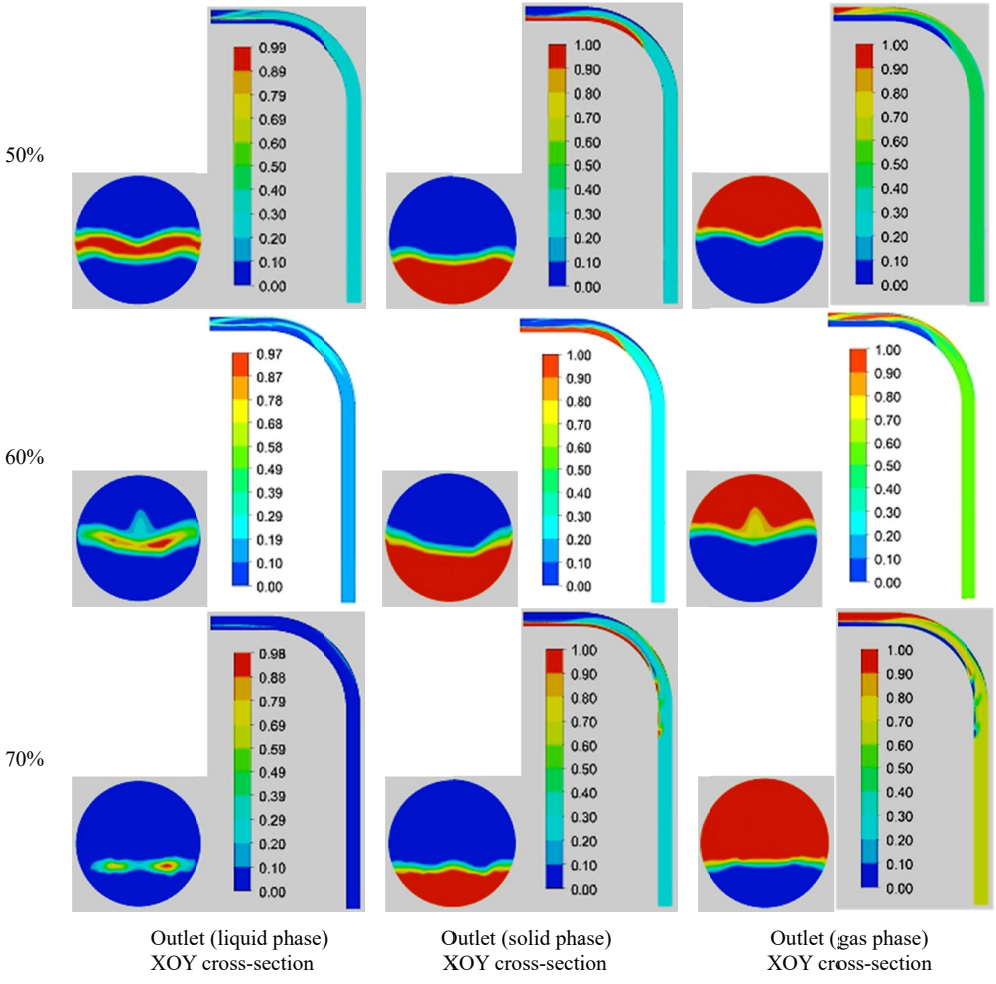

Fig. 15. XOY cross-section and volume score at exit when different gas volume fractions

3. Experimental research

3.1. Experimental Solutions

The experimental system adopts the deep-sea mining Yang experimental system of "deep-sea mineral resources development and utilisation of China's national key laboratory". The system has a vertical height of 30 m and a pipe diameter of 200 mm, allowing the hydro water transfer of 5000 m of undersea ore to be simulated by applying back pressure at the outlet. The chart diagram of the experimental platform is shown in Fig. 16.

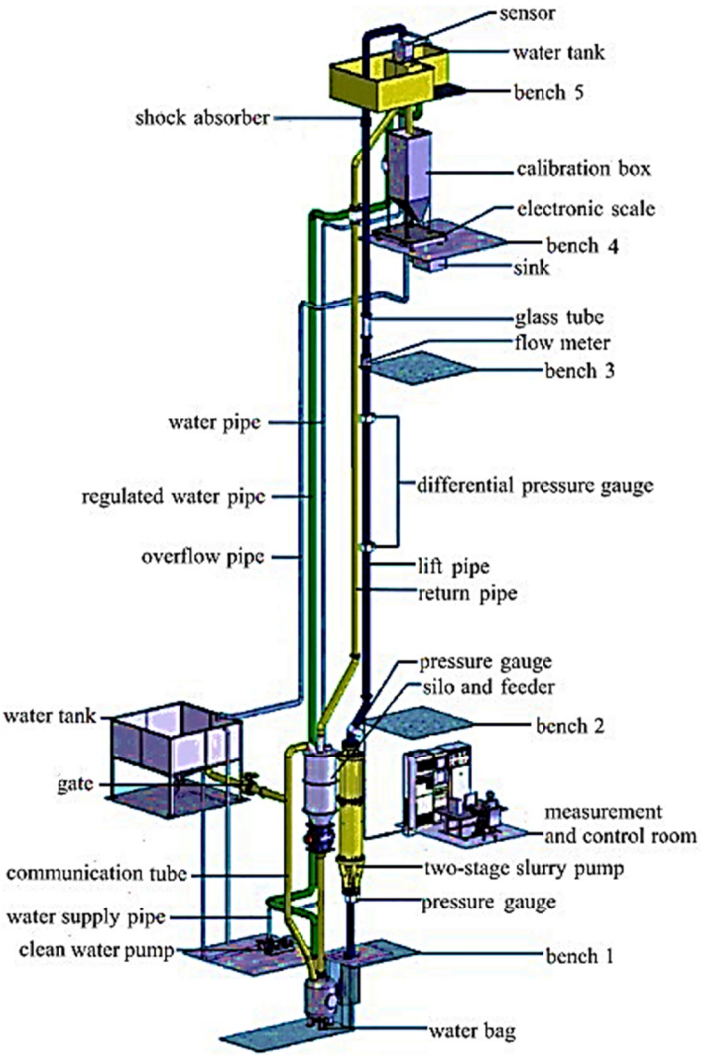

Fig. 16. Working principle of the experimental platform

Add the experimentally given nodule particles to the silo, fill the water tank with water, open the gate valve to fill the water package, and then start the two-stage slurry pump to extract the water from the water package into the lift pipe. Wait until the outlet of the pipeline is out of the water stability, adjust the variable frequency speed control box so that it is stable and stays in the required operating conditions and flow rate.

Start the feeder by adjusting the speed of the feeder to control the volume of the solid-phase particles at the bottom of the tube, to open the air pump adjustment flow at a certain speed into the middle of the pipeline gas. By observing the instrument data of the experimental system, it is adjusted to the required operating condition parameters.

3.2. Analysis of experimental results

Change the back pressure of the pipe outlet, and measure the pressure loss of 5 m above and below the glass pipe of the experimental system for each experiment. The experimental values and simulation results of pressure loss gradient at different tube inlet velocity is shown in Table 2.

TABLE 2

Pressure loss gradient at different tube inlet velocity

Working condition	Flow rate /(m/s)	Experimental value /(Pa/m)	Simulation value /(Pa/m)	Inaccuracy
The solid phase diameter is 20 mm, the solid phase volume fraction is 10%, and the gas phase volume fraction is 5%.	1.5	1499.68	1421.55	5.49%
	2	779.46	723.62	7.72%
	3	925.71	857.39	7.97%
	4	1088.83	1017.32	7.03%
	5	1222.64	1178.31	3.76%

It can be seen from the above experimental results that the experimental and simulation laws are consistent, and the relative error is small, all within 10%. This proves that the calculation model and simulation method used in this paper are feasible.

Fig. 17 is a line chart of the relationship between the gas phase volume fraction and the pipe pressure loss obtained by the numerical simulation and the experimental test at a speed of 3 m/s. From the figure, it can be seen that at a 20% volume score or more, the pressure loss is negative, the exit elbow section no longer has pressure loss, and at this point, the gas phase of the lift is larger. This shows that positive work done by the buoyancy of the gas phase is sufficient to counteract the negative effects done on each phase, such as friction. With the increase of gas-phase volume fraction, the gas phase buoyancy increases and the pressure loss of the pipe decreases gradually.

In addition, it can be seen from Fig. 17 that numerical simulation and the system pressure loss curve of experimental tests tend to change the law. Compared with numerical simulation, the pressure loss obtained by the experimental test is greater than the numerical simulation value, which is due to the numerical simulation, which does not take into account the friction loss of the system, the loss of kinetic energy caused by the collision of solid-phase particles, and the dissipation of thermodynamic energy.

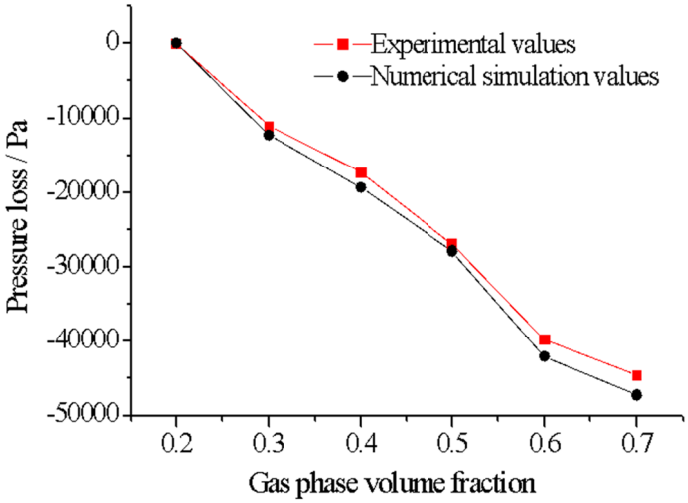

Fig. 17. Relationship between gas phase volume fraction and pressure loss

The natural gas hydrate is transported in the pipeline, and it automatically precipitates, the export gas phase volume fraction changes with the transmission rate, pipeline temperature pressure and other factors. The export gas production rate should be controlled so that the gas phase volume fraction is within 60% to ensure the stability of the system and the safety of exploitation.

4. Conclusions

The analysis of the part of the outlet bending pipe is obtained, the effect of the distribution of the phases in the curved pipe, including the ratio of bend diameter and gas-phase volume on the three-phase flow field in the pipe is obtained. The main conclusions are as follows:

(1) The three-phase flow in the tube is more uniformly distributed in each phase in the vertical stage, after the elbow, the liquid-phase is close to the pipe wall along the pipe flank to the outside of the pipe. A crescent-shaped formed and reached an angle of 45 degrees, the crescent-shaped liquid phase off the pipe wall was located close to the centre of the pipe and slowly moved horizontally. The solid phase is the shift along the pipe flank to the inside of the pipe, and when it is transferred to the inner centre, it begins to accumulate, gradually taking on the shape of an upright hill whilst growing shorter and wider. The gas phase shrinks along the flank of the pipe to the inner centre, then gathers toward the top of the solid phase, and finally passes through the liquid phase to the top of the horizontal pipe. Finally, the solid gas phase is layered.

(2) The maximum speed of each phase of the three-phase flow in the elbow is at the inside of the elbow from 45 to 60 degrees, and the distribution law of the speed along the axial direction of the pipe is about the same as the distribution law of the volume fraction. The velocity distribution along the radial path is affected by the secondary flow, and

the vortex core moves from the outside of the elbow to the inside of the elbow, which also affects the shape of the stacked solid-phase hill shape, the liquid-phase interface shape change and the shape of the gas-liquid interface. With the three-phase flow of transport, pressure reduction, bubble expansion, hydrate decomposition speed is accelerated, and the gas-phase volume fraction is naturally larger. The pressure loss will gradually decrease, the buoyancy of the gas-phase to the solid-liquid does positive work. When the gas phase volume fraction reaches 70%, there will be an obvious wall separation phenomenon, so it should be controlled within 60% to keep the system in a stable working state.

(3) At different pipe flow speeds, with the increase of the bending diameter ratio, the pressure loss of the elbow shows a generally decreasing trend. When the bend ratio is less than 5, it maintains a large pressure loss. When the bend ratio increases to 6, the pipe pressure loss decreases sharply, and after that, the pipe pressure loss decreases slowly as the bend ratio increases. The bend ratio is different as the pipe pressure loss is not consistent with the change of pipe flow speed. When the bend diameter ratio is 6, the pipe flow speed and pressure loss increase, but the change of magnitude of the pipe flow speed on the pipe pressure loss is very small.

Acknowledgements

This work was supported by the National Natural Science Foundation of China (51775561, 52006061), Natural Science fund of Hunan Province (2018JJ2522), Hunan Provincial Department of Education Project (20B327, 18A419); Hunan Province key research and development program (2019SK2192, 2020NK2063); Science and Technology Project of Hunan Provincial Water Resources Department (XSKJ2019081-56).

References

[1] Y.F. Makogon, S.A. Holditch, T.Y. Makogon, Natural gas-hydrates -a potential energy source for the 21st century. Journal of Petroleum Science & Engineering **56** (3), 14-31 (2007). DOI: https://doi.org/10.1016/j.petrol.2005.10.009

[2] H.L. Xu, W.Y. Kong, W.G. Hu, Analysis of influencing factors on suction capacity in seabed natural gas hydrate by cutter-suction exploitation. Journal of Central South University **25** (12), 2883-2895 (2018). DOI: https://doi.org/10.1007/s11771-018-3960-z

[3] L.Y. Shang, S.L. Zhao, Z. Pan, T.L. Huang, Study on Kinetic Characteristics of Solid-Liquid Two-Phase in Transporting Pipeline of Natural Gas Hydrate. Advanced Materials Research **91** (4), 1814-1818 (2014). DOI: https://doi.org/10.4028/www.scientific.net/AMR.881-883.1814

[4] A.V. Milkov, Worldwide distribution of submarine mud volcanoes and associated gas hydrates. Marine Geology **167** (2), 29-42 (2000). DOI: https://doi.org/10.1016/S0025-3227(00)00022-0

[5] M.K. Kareem, W.M. Abed, H.K. Dawood, Numerical simulation of hydrothermal behavior in a concentric curved annular tube. Heat Transfer **20** (49), 156-164 (2020). DOI: https://doi.org/10.1002/htj.21732

[6] Y.F. Makogon, Natural gas hydrates-A promising source of energy. Journal of Natural Gas Science and Engineering **2** (1), 49-59 (2010). DOI: https://doi.org/10.1016/j.jngse.2009.12.004

[7] N. Wei, W. Sun, Y. Meng, S. Zhou, Q. Li, Annular phase behavior analysis during marine natural gas hydrate reservoir drilling. Shiyou Xuebao/Acta Petrol Sinica **38** (6), 710-720 (2017). DOI: https://doi.org/10.7623/syxb201706011

[8] L. Jiang, N. Wei, J. Zhao, S. Zhou, K. Wu, The Experimental Simulation Technology and System of Solid Fluidization Exploitation of Marine Non-Diagenetic Natural Gas Hydrate. International Conference on Computational & Experimental Engineering and Sciences **21** (4), 81-83 (2019). DOI: https://doi.org/10.32604/icces.2019.04515

[9] S. Zhou, J. Zhao, Q. Li, W. Chen, J. Zhou, W. Na, Optimal design of the engineering parameters for the first global trial production of marine natural gas hydrates through solid fluidization. Natural Gas Industry B **5** (2), 118-131 (2018). DOI: https://doi.org/10.1016/j.ngib.2018.01.004

[10] S. Afzali, S. Zendehboudi, O. Mohammadzadeh, N. Rezaei, Hybrid mathematical modelling of three-phase flow in porous media: application to water-alternating-gas injection. Journal of Natural Gas Science and Engineering **4**, 103966 (2021). DOI: https://doi.org/10.32604/icces.2019.04515

[11] H. Li, S. Ma, Effect of thickness ratio of overlaying layer to hydrate bearing stratum upon the settlement of seabed sediments during natural gas hydrate dissociation. IOP Conference Series Earth and Environmental Science **526**, 012135 (2020). DOI: https://doi.org/10.32604/icces.2019.04515

[12] L. Li, H.L. Xu, F.Q. Yang, Three-phase flow of submarine gas hydrate pipe transport. Journal of Central South University **22** (9), 3650-3656 (2015). DOI: https://doi.org/10.1007/s11771-015-2906-y

[13] H.H. Zhan, H. Zhu, J.D. Chen, G. Wang, Numerical Simulation of Secondary Flow (Dean Vortices) in 90° Curved Tube. Boiler Technology **41** (4), 45-54 (2010). DOI: https://doi.org/10.1016/j.ces.2018.10.029

[14] X. Su, W. Gao, X. Liu, C. Xie, B. Xu, Numerical simulation of a three-dimensional flow field in compact spinning with a perforated drum: Effect of a guiding device. Textile Research Journal **83** (19), 2093-2108 (2013). DOI: https://doi.org/10.1177/0040517513483859

[15] C.A. Koh, Towards a fundamental understanding of natural gas hydrates. Chemical Society Reviews **31** (3), 157-167 (2002). DOI: https://doi.org/10.1039/b008672j

[16] M.T. Reshma, M. Kumar, L. Rao, Numerical modelling of oxygen mass transfer in diffused aeration systems: A CFD-PBM approach. Journal of Water Process Engineering **40**, 101920. DOI: https://doi.org/10.1016/j.jwpe.2021.101920

[17] T. Wang, J. Wang, J. Yong, A CFD-PBM coupled model for gas-liquid flows. Aiche Journal **52** (1), 125-140 (2010). DOI: https://doi.org/10.1002/aic.10611

[18] S.Z. Kassab, H.A. Kandil, H.A. Warda, Experimental and analytical investigations of airlift pumps operating in three-phase flow. Chemical Engineering Journal **131** (3), 273-281 (2007). DOI: https://doi.org/10.1016/j.cej.2006.12.009

[19] H. Kato, T. Miyazawa, S. Timaya, A study of an air-lift pump for solid particles. Jsme International Journal **18** (117), 286-294 (2008). DOI: https://doi.org/10.1299/jsme1958.18.286

[20] X. Yin, I. Zarikos, N.K. Karadimitriou, A. Raoof, S.M. Hassanizadeh, Direct Simulations of Two-phase Flow Experiments of Different Geometry Complexities Using Volume-of-Fluid (VOF) Method. Chemical Engineering Science **43** (2), 112-123 (2018). DOI: https://doi.org/10.1016/j.ces.2018.10.029